



OPEN ACCESS

EDITED BY

Arianna Giorgetti,
University of Bologna, Italy

REVIEWED BY

Jennifer Pascali,
University of Padua, Italy
Dino Luethi,
University Hospital of
Basel, Switzerland
Jeremy Carlier,
Sapienza University of Rome, Italy

*CORRESPONDENCE

Adam Ametovski
adam.ametovski@sydney.edu.au
Samuel D. Banister
samuel.banister@sydney.edu.au

[†]These authors have contributed
equally to this work and share senior
authorship

SPECIALTY SECTION

This article was submitted to
Psychopharmacology,
a section of the journal
Frontiers in Psychiatry

RECEIVED 03 August 2022

ACCEPTED 24 August 2022

PUBLISHED 28 September 2022

CITATION

Sparkes E, Boyd R, Chen S,
Markham JW, Luo JL, Foyzun T,
Zaman H, Fletcher C, Ellison R,
McGregor IS, Santiago MJ, Lai F,
Gerona RR, Connor M, Hibbs DE,
Cairns EA, Glass M, Ametovski A and
Banister SD (2022) Synthesis and
pharmacological evaluation of newly
detected synthetic cannabinoid
receptor agonists AB-4CN-BUTICA,
MMB-4CN-BUTINACA,
MDMB-4F-BUTICA,
MDMB-4F-BUTINACA and their
analogs. *Front. Psychiatry* 13:1010501.
doi: 10.3389/fpsy.2022.1010501

COPYRIGHT

© 2022 Sparkes, Boyd, Chen,
Markham, Luo, Foyzun, Zaman,
Fletcher, Ellison, McGregor, Santiago,
Lai, Gerona, Connor, Hibbs, Cairns,
Glass, Ametovski and Banister. This is
an open-access article distributed
under the terms of the [Creative
Commons Attribution License \(CC BY\)](https://creativecommons.org/licenses/by/4.0/).
The use, distribution or reproduction
in other forums is permitted, provided
the original author(s) and the copyright
owner(s) are credited and that the
original publication in this journal is
cited, in accordance with accepted
academic practice. No use, distribution
or reproduction is permitted which
does not comply with these terms.

Synthesis and pharmacological evaluation of newly detected synthetic cannabinoid receptor agonists AB-4CN-BUTICA, MMB-4CN-BUTINACA, MDMB-4F-BUTICA, MDMB-4F-BUTINACA and their analogs

Eric Sparkes^{1,2}, Rochelle Boyd^{1,3}, Shuli Chen⁴,
Jack W. Markham^{1,2,5}, Jia Lin Luo^{1,3}, Tahira Foyzun⁶,
Humayra Zaman⁶, Charlotte Fletcher^{1,3}, Ross Ellison⁷,
Iain S. McGregor^{1,3}, Marina J. Santiago⁶, Felcia Lai⁵,
Roy R. Gerona⁷, Mark Connor⁶, David E. Hibbs⁵,
Elizabeth A. Cairns^{1,3}, Michelle Glass⁴, Adam Ametovski^{1,2*†} and
Samuel D. Banister^{1,2*†}

¹The Lambert Initiative for Cannabinoid Therapeutics, Brain and Mind Centre, The University of Sydney, Sydney, NSW, Australia, ²Faculty of Science, School of Chemistry, The University of Sydney, Sydney, NSW, Australia, ³Faculty of Science, School of Psychology, The University of Sydney, Sydney, NSW, Australia, ⁴Department of Pharmacology and Toxicology, University of Otago, Dunedin, New Zealand, ⁵Faculty of Medicine and Health, School of Pharmacy, The University of Sydney, Sydney, NSW, Australia, ⁶Macquarie Medical School, Macquarie University, Sydney, NSW, Australia, ⁷Clinical Toxicology and Environmental Biomonitoring Laboratory, University of California, San Francisco, San Francisco, CA, United States

Synthetic cannabinoid receptor agonists (SCRAs) continue to make up a significant portion new psychoactive substances (NPS) detected and seized worldwide. Due to their often potent activation of central cannabinoid receptors *in vivo*, use of SCRAs can result in severe intoxication, in addition to other adverse health effects. Recent detections of AB-4CN-BUTICA, MMB-4CN-BUTINACA, MDMB-4F-BUTICA and MDMB-4F-BUTINACA mark a continuation in the appearance of SCRAs bearing novel tail substituents. The proactive characterization campaign described here has facilitated the detection of several new SCRAs in toxicological case work. Here we detail the synthesis, characterization, and pharmacological evaluation of recently detected SCRAs, as well as a systematic library of 32 compounds bearing head, tail, and core group combinations likely to appear in future. *In vitro* radioligand binding assays revealed most compounds showed moderate to high affinity at both CB₁ (pK_i = < 5 to 8.89 ± 0.09 M) and CB₂ (pK_i = 5.49 ± 0.03 to 9.92 ± 0.09 M) receptors. *In vitro* functional evaluation using a fluorescence-based membrane potential assay showed that most compounds were sub-micromolar to sub-nanomolar agonists at CB₁ (pEC₅₀ = < 5 to 9.48 ± 0.14 M) and CB₂ (pEC₅₀ = 5.92 ± 0.16 to 8.64 ± 0.15 M)

receptors. An *in silico* receptor-ligand docking approach was utilized to rationalize binding trends for CB₂ with respect to the tail substituent, and indicated that rigidity in this region (i.e., 4-cyanobutyl) was detrimental to affinity.

KEYWORDS

synthetic cannabinoid, cannabinoid receptor 1 agonists, pharmacology, cannabinoids, SCRA, docking, *in vitro* evaluation, synthesis

Introduction

Synthetic cannabinoid receptor agonists (SCRAs) represent a large portion of detected new psychoactive substances (NPS) globally, accounting for 29% of the 1,047 NPS identified between 2009 and 2019 (1). Commonly sold as herbal blends, such as “Spice,” “K2,” and “Black Mamba” which are consumed by smoking, SCRAs are part of a conscious effort by manufacturers and retailers to mimic the effect of Δ^9 -tetrahydrocannabinol (THC, **1**, Figure 1), the primary intoxicating compound in cannabis (2–6). Several mass intoxication events have been observed over the past decade, with clinically significant impact on patients including psychosis, seizure, respiratory failure, encephalopathy, necrotizing pancreatitis, acute kidney injury, and death (3, 7–31).

SCRAs primarily target the endocannabinoid system, specifically as agonists of centrally expressed cannabinoid 1 receptors (CB₁), to provide users with a high analogous to cannabis, although these compounds generally display equal or better affinity and potency at CB₁ compared with THC. However, unlike THC, SCRAs such as JWH-018 (2), MDMB-FUBINACA (3), and ADB-BUTINACA (4) generally act as high efficacy agonists at CB₁ resulting in significantly greater intoxication of users, and display differing profiles of tolerance, dependence, and withdrawal (32).

Modern SCRAs typically consist of amino acid-derived indole- and indazole-3-carboxamide type scaffolds, similar to compounds disclosed by Pfizer in a series of patents in 2009 (33–38). Appearance of NPS containing modification of these scaffolds has seemingly been a result of incoming legislation bringing detected compounds under national and international control, while attempting to retain CB₁ activity. Recent approaches observed include scaffold hopping, fluorination, nitrogen walking, alkyl chain contraction, and homologation, as well as the coupling of different amino acid residues to the substituted heterocyclic cores. These modifications have led

to a significant structural evolution of contemporary SCRAs from the late 2000s, with equivalent or increased potency at CB₁ (39–41).

The utility of proactive synthesis programs to detect emerging NPS has recently facilitated the detection of two new SCRAs bearing the 4-cyanobutyl tail moiety. The indole and indazole derivatives AB-4CN-BUTICA (5) and MMB-4CN-BUTINACA (6, a.k.a. AMB-4CN-BUTINACA), respectively, were identified in Alabama, facilitated by proactive reference standard generation and toxicological screening by our laboratories (Figure 2) (42, 43). The 4-fluorobutyl compounds MDMB-4F-BUTICA (7) and MDMB-4F-BUTINACA (8) were also recently detected, with the latter involved in a suicide, as well as multiple fatal intoxications (7, 31, 44–49). With the appearance of these compounds, it is feasible that NPS manufacturers may introduce the 4-fluorobutyl or 4-cyanobutyl subunits to other amino acid-derived indole-, indazole- and 7-azaindole-3-carboxamide SCRAs in future. As such, this paper describes the synthesis, chemical analysis, and pharmacological characterization of the newly detected SCRAs, as well as a series of 32 systematic analogs (5–40, Figure 3). Due to the combinatorial design of the library, direct comparison of the contributions of subunits to the pharmacological profile of the compounds enabled identification of key structure-activity relationships (SARs). *In vitro* binding and functional data were obtained at both CB₁ and CB₂, and an *in silico* docking approach was utilized to explore observed SARs, especially concerning differences in binding between 4-cyanobutyl and 4-fluorobutyl tail moieties. Most compounds displayed high affinity, potency, and efficacy at both CB₁ and CB₂, suggesting these compounds should be included in NPS monitoring programs. Given the similarity in structure and pharmacological profile of the library evaluated in this work compared to existing SCRAs, these data provide important insights into the potential effect of these compounds in humans, pending evaluation *in vivo*.

Experimental

General chemical synthesis details

All reactions were performed under an atmosphere of nitrogen unless otherwise specified. Methyl 1*H*-indazole-3-carboxylate (**42**) and methyl 1*H*-pyrrolo[2,3-*b*]pyridine-3-carboxylate (**43**) were purchased from Fluorochem LTD (Derbyshire, UK) and used as received. 1-Ethyl-3-(3-dimethylaminopropyl)carbodiimide hydrochloride (EDC•HCl) was purchased from Oakwood Chemical (Estill, SC, USA). Deuterated solvents (CD₃OD, CDCl₃, and DMSO-*d*₆) were purchased from Cambridge Isotope Laboratories (Tewksbury, MA, USA). Unless otherwise stated, all other reagents and solvents used for this manuscript were obtained from Sigma-Aldrich/Merck (Castle Hill, NSW, Australia) and used as purchased. Analytical thin-layer chromatography was performed using Merck aluminum-backed silica gel 60 F254 (0.2 mm) plates (Merck, Darmstadt, Germany), which were visualized using shortwave (254 nm) UV fluorescence. Flash chromatography was performed using a Biotage Isolera Spektra One and Biotage SNAP KP-Sil silica cartridges (Uppsala, Sweden), with gradient elution terminating at the solvent combination indicated for each compound (*vide infra*). Melting point ranges (m.p.) were measured in open capillaries using a Stuart SMP50 Automated melting point apparatus (Cole-Palmer, Staffordshire, UK) and are uncorrected. Nuclear magnetic resonance (NMR) spectra were recorded at 298 K using an Agilent 400-MHz spectrometer (Santa Clara, CA, USA), or a Bruker NEO 300 MHz NMR spectrometer (Billerica, MA, USA). The data are reported as chemical shift (δ ppm) relative to the residual protonated solvent resonance, relative integral, multiplicity (s = singlet, brs = broad singlet, d = doublet, t = triplet, q = quartet, quin = quintet, m = multiplet), coupling constants (*J* Hz), and assignment. High resolution mass spectrometry (HRMS) data were collected using an Agilent LC 1260-QTOF/MS 6550 (Santa Clara, CA, US) or a Bruker Solarix 2xR 7T Fourier Transform Ion Cyclotron Resonance Mass Spectrometer. A methanolic extract of each pure standard was run using an electrospray ionization (ESI) source in automated MS/MS (information dependent acquisition) mode. Accurate mass for the parent ion and its corresponding mass error expressed in parts per million (ppm) are reported. LC-MS/UV data were acquired using a Shimadzu (Kyoto, Japan) Nexera LC-30AD UHPLC system coupled to a Shimadzu SPD-20AV photo diode array detector and a Shimadzu LCMS-8040 triple-quadrupole mass spectrometer, equipped with an electrospray ionization (ESI) source. Compounds were dissolved in a 90:10 mixture of 0.1% formic acid in water and methanol, and placed in the UHPLC autosampler that was maintained at 8°C. Elution was performed in gradient mode with an Agilent (CA, USA) Zorbax XDB-C18 column (2.1 × 50 mm, 3.5 μ m particle size), held at 50°C, with a 10 μ L injection volume. The

mobile phases were 0.1% formic acid in water (A) and methanol (B). Mobile phase composition was held at 10% B until 0.5 min, then steadily increasing to 100% B at 2.5 min, holding until 3 min, and then re-equilibrating at 10% B for a total run time of 4 min. UV absorbance was measured from 190 to 800 nm. UV data from blank injections were subtracted to account for mobile phase absorbance and background noise. Single stage mass spectra (MS1) were collected in positive ESI mode using a single quadrupole (Q3) scanning from *m/z* 100–600. All data were processed using Shimadzu LabSolutions (v 5.89) software. Fourier-transform infrared spectroscopy (FTIR) spectra were collected using a Bruker Alpha II ATR FTIR spectrophotometer. Precursors **44–51**, and compounds **6**, **7**, **11**, **17**, and **22** were synthesized and used as is, as previously described (50, 51). Synthetic procedures and characterization data (¹H and ¹³C NMR, melting point, *R_f*, FTIR, HRMS, UV, and LCMS) can be found in the supporting information.

In vitro binding evaluation

Human embryonic kidney (HEK) cells expressing either human CB₁ receptors N-terminally tagged with pplss (preprolactin signal sequence) and 3HA (3x haemagglutinin) epitopes or human CB₂ receptor N-terminally tagged with 3HA were harvested in 5 mM EDTA in PBS, and “P2” membranes were prepared in sucrose buffer as previously described (52, 53). Protein content was estimated using a BioRad (Hercules, CA) DC protein assay (modified Lowry assay). For binding assays, radioligand ([³H]-CP55,940, PerkinElmer, Waltham, MA, USA), non-radiolabeled drugs, and P2 membrane preparations were diluted in binding buffer (50 mM HEPES pH 7.4, 1 mM MgCl₂, 1 mM CaCl₂, 2 mg/mL NZ-origin BSA, MP Biomedicals, Santa Ana, CA, USA) and dispensed into 96-well, polypropylene V-well plates (Hangzhou Gene Era Biotech Co Ltd, Zhejiang, China) in a final reaction volume of 200 μ L (membranes were dispensed last). Final radioligand concentration was 1 nM for all assays. Protein content was 3 μ g/point for pplss-3HA-hCB₁ HEK membranes, and 2 μ g/point for 3HA-hCB₂ HEK membranes for the assays using type A harvest plate (PerkinElmer, GF/C filters, 1.2 μ m pores), these plates were discontinued during the course of this study, and replaced with type B harvest plates (Merk Millipore, GF/C filters, 1.2 μ m pores). As these plates appear to retain a smaller proportion of the protein, membrane content was increased to 8 μ g/point for CB₁ membranes, and 3 μ g/point for CB₂ membranes. When all components had been dispensed, the V well plate was sealed and incubated for 1 h at 30°C. During the incubation, the 96 well harvest plate was treated with 0.1% w/v branched polyethyleneimine (PEI; Sigma Aldrich) in H₂O. Immediately prior to washing, PEI was washed through the filters using a vacuum manifold (Pall Corporation, Port Washington, NY) and all wells were washed once with ice cold

wash buffer (50 mM HEPES pH 7.4, 500 mM NaCl, 1 mg/mL BSA). Equilibrated binding mixture was then transferred to the harvest plate under vacuum, and samples washed through. For the assays using type A harvest plate, binding wells were rinsed once with wash buffer and transferred to the harvest plate, and then wells were washed three more times with 200 μ L of wash buffer. The plate was then removed, and filters allowed to dry overnight. The next day, the plate bottom was sealed, and 50 μ L of Ultima Gold XR scintillation fluid (PerkinElmer) was dispensed to each well and the plate loaded into the 96 well “rigid” cassette. For the assays using type B harvest plate, samples were rapidly washed 4 times with 100 μ L of wash buffer. The bottom of the plate was then removed, and filters allowed to dry overnight. The next day, the plate was inserted into a 96 well “rigid” cassette. The base of the cassette was sealed and 50 μ L of scintillation fluid was added to each well. The top of the plates were sealed prior to loading into a Wallac MicroBeta2[®] TriLux Liquid Scintillation Counter (PerkinElmer). Scintillation was detected after a 30 min delay, for 2 min per well. Counts were corrected for detector efficiency. Data were then exported and analyzed in GraphPad Prism v9 (GraphPad Software Inc., La Jolla, CA, USA). K_i was determined through fit of “Competition binding- One site fit K_i ” in GraphPad prism using a K_d of 3.50 nM for the radioligand for the assays using type A harvest plate; while for the assays using harvest plate B, K_d was 3.58 nM for binding at CB₁ and 1.162 nM for binding at CB₂ (K_d was determined empirically using homologous competition assay under matching conditions). Log K_i were determined for at least three independent experiments (maximum 6) and combined to determine mean $pK_i \pm$ SEM reported in Tables 1, 2. Assays for compounds 5, 6, 10–12, 14, 15, 17, 18, 20–22, 24, 29, 34 used type A harvest plate. Assays for compounds 7–9, 13, 16, 19, 23, 25–28, 30–33, 35–40 used type B harvest plates.

In vitro functional evaluation

Mouse AtT20 FlpIn adenocarcinoma cells stably transfected with human CB₁ or CB₂ were cultured in DMEM containing 10% FBS, 100 U penicillin/streptomycin, and 80 μ g/mL of hygromycin, as previously described (54). Cells were passaged at 80% confluency, cells for assays were grown in 75 cm² flasks and used at 90% confluence. The day before the assay cells were detached from the flask with trypsin/EDTA (Sigma Aldrich) and resuspended in 10 mL of Leibovitz’s L-15 media (L-15) supplemented with 1% FBS, 100 U penicillin/streptomycin, and 15 mM glucose. The cells were plated in volume of 90 μ L in black walled, clear bottomed 96-well microplates (Corning, Corning, NY, USA) and incubated overnight at 37°C in ambient CO₂. Membrane potential was measured using a Membrane Potential Assay Kit (blue) from Molecular Devices (San Jose, CA, USA), as described previously (55, 56). The dye was reconstituted with assay buffer [145 mM NaCl, 22 mM HEPES,

0.338 mM Na₂HPO₄, 4.17 mM NaHCO₃, 0.441 mM KH₂PO₄, 0.407 mM MgSO₄, 0.493 mM MgCl₂, 1.26 mM CaCl₂, 5.56 mM glucose (pH 7.4)]. Prior to the assay, cells were loaded with 90 μ L/well of the dye solution without removal of the L-15. Plates were then incubated at 37°C in ambient CO₂ for 60 min. Fluorescence was measured using a FlexStation 3 (Molecular Devices) microplate reader with cells excited at a wavelength of 530 nm and emission measured at 565 nm. Baseline readings were taken every 2 s for at least 2 min, at which time either drug or vehicle was added in a volume of 20 μ L. The background fluorescence of cells without dye or dye without cells was negligible. Changes in fluorescence were expressed as a percentage of baseline fluorescence after subtraction of the changes produced by vehicle (DMSO, final concentration was no more than 0.1%) addition. Concentration-response data were analyzed using GraphPad Prism 9 (GraphPad Software, San Diego, CA, USA), using a four-parameter non-linear regression to fit concentration-response curves on data from 3 to 6 independent experiments.

Molecular modeling

Protein preparation

The cryo-EM structures of the CB₁ receptor (PDB: 6N4B) and the CB₂ receptor (PDB: 6KPF) were retrieved from RCSB PDB (57–59). The structures were prepared with Maestro’s Protein Preparation Wizard as follows (60). The G proteins and cholesterol were removed, leaving only the CB₁ and CB₂ receptor and their cognate ligands. The preparation process consisted of assigning bond orders, adding hydrogens, generation of disulfide bonds, generation of missing side chains using Prime, generating het states using Epik at pH 7.4 \pm 1.0, and deleting water molecules beyond 3 Å from het groups (61, 62). The hydrogen bonding network was optimized, the pK_a values of the protein were predicted using PROPKA, and target pH value was set at 7.4 (63). Lastly, the protein structure was minimized using the OPLS4 force field where RMSD of the atom displacement for terminating the minimization was set as 0.3 Å (64).

Ligand preparation

Ligands were prepared using LigPrep to generate energy minimized 3D structures (65). OPLS4 force field was used for minimization. Epik was used to generate all possible ionized states at pH 7.4 \pm 1.0.

Ligand docking

A receptor grid was generated using Glide, with a van der Waals radius scaling factor of 1.0 and a partial charge cutoff at 0.25 (66). The binding site was defined by the centroid

of the cognate ligand for each structure. The Van der Waals scaling factor for the ligands was set to 0.80 with a partial charge cut-off at 0.15. The precision was set to Extra Precision (XP) with flexible ligand sampling. Nitrogen inversions and ring conformations were sampled and Epik state penalties were added to the docking scores. The ligand cores were restricted to the position of the cognate ligand by their maximum common substructure and post docking minimization was performed. Poses that had the lowest RMSD between the 4-fluorobutyl and 4-cyanobutyl analogs were taken for direct comparison.

Strain calculations

The internal strain of ligands in their bound and unbound states was calculated using MacroModel (65). The 4RDDD solvation forcefield was used, a constant 4.00 kcal/mol energy offset selected, a penalty scale factor of 0.25 and Cartesian restraints with a bound state half-width of 0.3 Å and a 120 kcal/mol/Å² force constant.

Binding site mapping

The binding site regions for both the CB₁ and CB₂ structures were evaluated using SiteMap (67). SiteMap was run in evaluate mode using the structures cognate ligand and a 5 Å buffer. A minimum of 15 site points per binding site was set, using the “more restrictive” definition of hydrophobicity and a standard grid. Site maps were cropped at 4 Å from the nearest site point.

Results and discussion

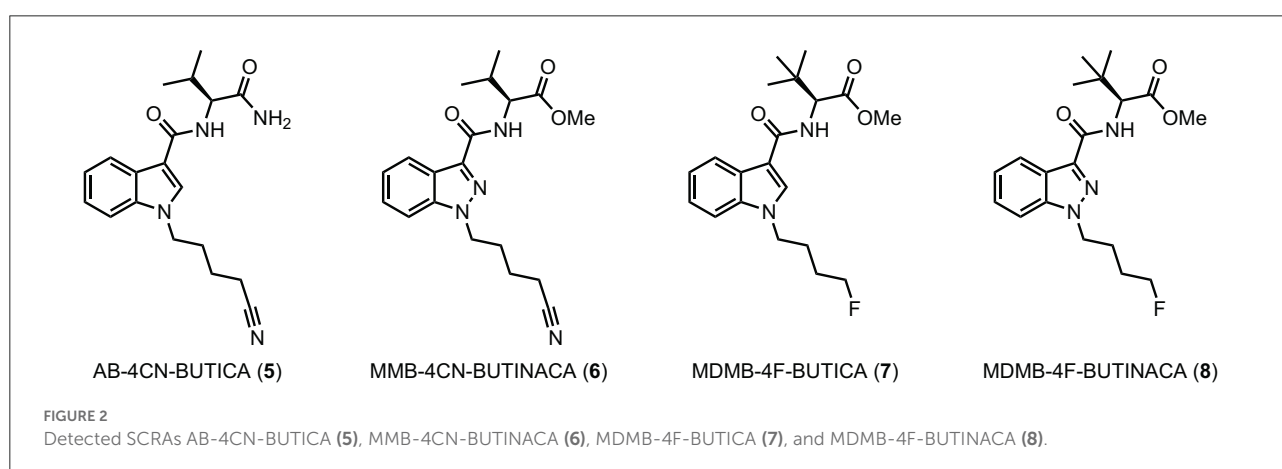
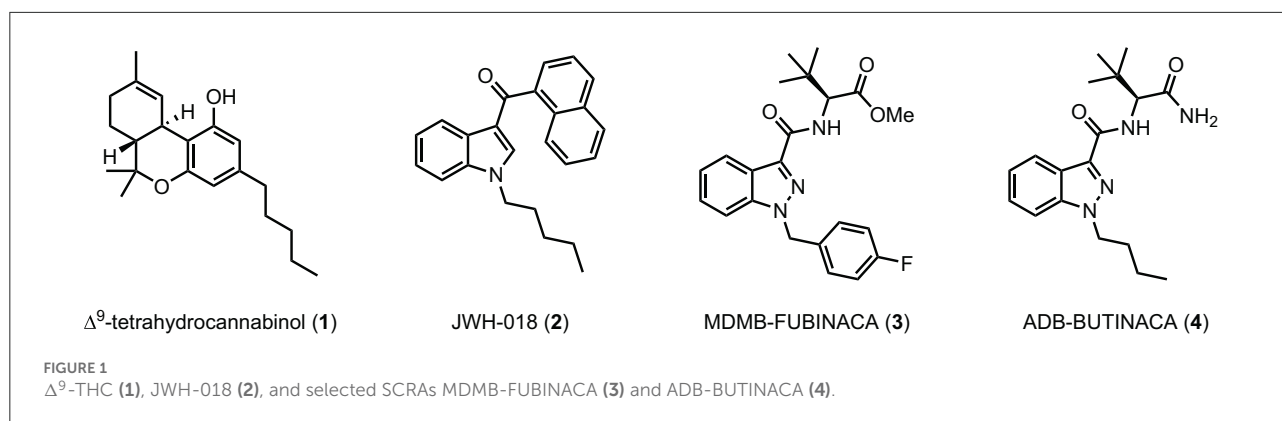
Synthesis

Indole-based SCRA were derived from indole (41), with a convenient one-pot alkylation and trifluoroacetylation procedure employed to give intermediate *N*-alkyl-5-(3-(2,2,2-trifluoroacetyl)-1*H*-indoles before subsequent hydrolysis gave *N*-alkyl-1*H*-indole-3-carboxylic acids 44 and 45 in good yield (Scheme 1, eq. 1). This was then subjected to 1-ethyl-3-(3-dimethylaminopropyl)carbodiimide (EDC)/1-hydroxybenzotriazole (HOBt)-mediated amide coupling with the appropriate amino acid derivatives to furnish the final indole derived compounds (5, 7, 9, 10, 17–19, 25–27, 34, 35). The indazole and 7-azaindole derivatives were synthesized using a similar sequence from methyl indazole- or methyl-7-azaindole-3 carboxylates 42 and 43 (Scheme 1, eq. 2). Thus, alkylation with the appropriate alkylbromide and sodium hydride provided methyl *N*-alkyl-indazole- or methyl *N*-alkyl-7-azaindole-3 carboxylates 46–49 before hydrolysis to give the corresponding carboxylic acids 50–53. In the same manner as described previously, EDC/HOBt-mediated

amide coupling furnished *N*-alkyl-indazole- or -alkyl-7-azaindole-3-carboxylamides 6, 8, 11–16, 20–24, 28–33, 36–40 (6, 50, 51, 54, 68, 69). Synthetic procedures and characterization data (¹H and ¹³C NMR, melting point, R_f, FTIR, HRMS, and LCMS) for all novel compounds can be found in the supporting information.

In vitro binding affinity trends for 5–40

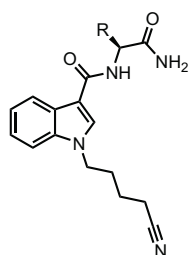
Following our previous efforts in the characterization of existing SCRA, *in vitro* binding data were obtained via a competitive radio binding assay in HEK293 cells stably transfected with human cannabinoid receptor 1 (hCB₁) or human cannabinoid receptor 2 (hCB₂) (6, 50, 54, 68, 69). Ligand affinity (pK_i) was determined based on extent to which compounds displaced the tritiated standard [³H]CP55,940 (Tables 1, 2). Except for terminal amide bearing 7-azaindoles SCRA 38, 33 and 16, all compounds displayed micromolar to sub-nanomolar affinity for CB₁ receptors (pK_i = 8.89 ± 0.09–5.48 ± 0.11). Similar or increased CB₂ affinity was observed in almost all cases (pK_i = 9.92 ± 0.09–5.49 ± 0.03), with several examples exhibiting sub-nanomolar affinities for this receptor subtype (20, pK_i = 9.53 ± 0.07; 29, pK_i = 9.16 ± 0.04; 7, pK_i = 9.30 ± 0.12; 8, 9.92 ± 0.09; 37, pK_i = 9.34 ± 0.05), which represent the highest affinities in the series. Across the 4-cyanobutyl and 4-fluorobutyl tail substituents, no clear trend was apparent for CB₁ except within methyl *tert*-leucinate (18, 20, 23 > 7, 8, 39) and methyl phenylalaninate (35, 37, 40 > 19, 21, 24) subgroups, whereby 4-cyanobutyl and 4-fluorobutyl substitution, respectively, conveyed increased affinity, albeit slightly. Only 4-cyanobutyl bearing 15 (CB₁ pK_i = 6.81 ± 0.09) showed affinity an order of magnitude greater than its 4-fluorobutyl analog 32 (CB₁ pK_i = 5.90 ± 0.06). Conversely, 4-fluorobutyl derivatives were in general equal or better ligands at CB₂. Variation of the headgroup within the indazole series (AB: 28 > 11; ADB: 29 > 12; APP: 30 > 13; MMB: 36 > 4; MDMB: 8 ≈ 20; MMP: 37 ≈ 21) highlights this trend. A clear structure-affinity trend within the core scaffold was observed, with indazoles (CB₁, pK_i = 8.89 ± 0.09–5.48 ± 0.11; CB₂, pK_i = 9.53 ± 0.07–6.78 ± 0.03) providing the best affinity to both CB₁ and CB₂, followed closely by indoles (CB₁, pK_i = 8.18 ± 0.11–5.50 ± 0.10; CB₂, pK_i = 9.30 ± 0.12–6.22 ± 0.13). Finally, 7-azaindoles (CB₁, pK_i = 8.03 ± 0.13–< 5; CB₂, pK_i = 8.67 ± 0.07–5.49 ± 0.03) exhibited reduced affinity compared with the other groups, often by an order of magnitude. This is in keeping with previous studies detailing related indole, indazole and 7-azaindole carboxamides (36, 51, 54). Notably, the indazole core was required to achieve sub-nanomolar affinity for CB₂ (i.e., 20, 29, 8, 37) except in the case of 7, whereby high affinity was maintained with combination of an indole core, and importantly, the methyl *tert*-leucinate head group. In each core and tail sub-group, the *tert*-leucine



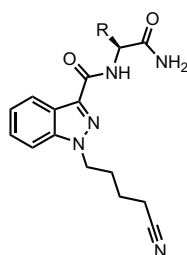
derivatives (MDMB > ADB) were consistently the best ligands for both CB₁ and CB₂, followed by phenylalanine methyl esters (MPP), which were better than both valine derivatives (MMB > AB), and finally, phenylalaninamides (APP). For example, within the indole set, a *tert*-leucinate conferred the highest CB₁ affinity (18, pK_i = 8.18 ± 0.11), which was reduced by an order of magnitude for the corresponding phenylalaninate (19, pK_i = 7.07 ± 0.09), and further halved for valine derivatives (17, pK_i = 6.80 ± 0.14). An alternate order was observed for the corresponding terminal amides of *tert*-leucine (9, pK_i = 8.17 ± 0.12), valine (5, pK_i = 6.26 ± 0.09) and phenylalanine (10, pK_i = 5.48 ± 0.11), which conferred one of the lowest affinities in the set. Affinities for CB₂ followed the same general trend, although phenylalaninamides exhibited affinities up to an order of magnitude greater compared to CB₁ (e.g., 13, CB₁ pK_i = 5.48 ± 0.11; CB₂ pK_i = 6.78 ± 0.03). Indeed, APP derivatives were not well-tolerated at CB₁ and thus modest selectivity for CB₂ (4- to 50-fold) was observed in this class (i.e., 10, 33, 16, 27, 30).

In vitro CB₁ and CB₂ functional characterization of 5–40

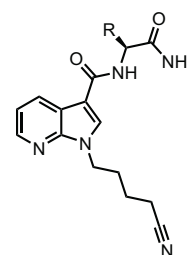
SARs for compounds 5–40 were also investigated *via* a fluorescence-based functional assay using AtT20 cells transfected with hCB₁ and hCB₂. This method measures change in membrane potential resulting from G_{βγ}-coupled activation of inwardly rectifying potassium channels (GIRKs). The full concentration-response curves of 5–40 are shown in Figure 4, with potencies and efficacies referenced to 1 μM CP55,940 in Tables 1, 2. Most compounds, except for selected phenylalaninamide and/or 7-azaindole derivatives (10, 13, 16, 27, 33, and 38), had maximal efficacy (E_{max} = 102–122%), and exhibited nanomolar to sub-nanomolar potencies (pEC₅₀ = 9.48 ± 0.14–6.30 ± 0.05) at CB₁. In general, this group activated CB₂ with equal or increased potency (pEC₅₀ = 8.67 ± 0.17–6.41 ± 0.10) and efficacy, albeit, with no ligands active at sub-nanomolar levels. As with other SCRA, these compounds are generally similar or greater potency, but more efficacious than



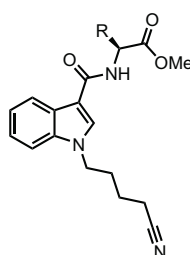
AB-4CN-BUTICA (5: $\text{R} = \text{CH}(\text{CH}_3)_2$)
 ADB-4CN-BUTICA (9: $\text{R} = \text{C}(\text{CH}_3)_3$)
 APP-4CN-BUTICA (10: $\text{R} = \text{CH}_2\text{Ph}$)



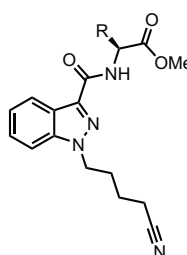
AB-4CN-BUTINACA (11: $\text{R} = \text{CH}(\text{CH}_3)_2$)
 ADB-4CN-BUTINACA (12: $\text{R} = \text{C}(\text{CH}_3)_3$)
 APP-4CN-BUTINACA (13: $\text{R} = \text{CH}_2\text{Ph}$)



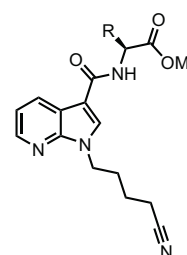
AB-4CN-BUT7AICA (14: $\text{R} = \text{CH}(\text{CH}_3)_2$)
 ADB-4CN-BUT7AICA (15: $\text{R} = \text{C}(\text{CH}_3)_3$)
 APP-4CN-BUT7AICA (16: $\text{R} = \text{CH}_2\text{Ph}$)



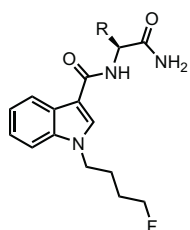
MMB-4CN-BUTICA (17: $\text{R} = \text{CH}(\text{CH}_3)_2$)
 MDMB-4CN-BUTICA (18: $\text{R} = \text{C}(\text{CH}_3)_3$)
 MPP-4CN-BUTICA (19: $\text{R} = \text{CH}_2\text{Ph}$)



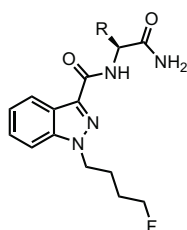
MMB-4CN-BUTINACA (6: $\text{R} = \text{CH}(\text{CH}_3)_2$)
 MDMB-4CN-BUTINACA (20: $\text{R} = \text{C}(\text{CH}_3)_3$)
 MPP-4CN-BUTINACA (21: $\text{R} = \text{CH}_2\text{Ph}$)



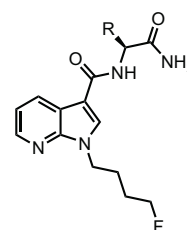
MMB-4CN-BUT7AICA (22: $\text{R} = \text{CH}(\text{CH}_3)_2$)
 MDMB-4CN-BUT7AICA (23: $\text{R} = \text{C}(\text{CH}_3)_3$)
 MPP-4CN-BUT7AICA (24: $\text{R} = \text{CH}_2\text{Ph}$)



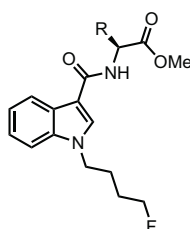
AB-4F-BUTICA (25: $\text{R} = \text{CH}(\text{CH}_3)_2$)
 ADB-4F-BUTICA (26: $\text{R} = \text{C}(\text{CH}_3)_3$)
 APP-4F-BUTICA (27: $\text{R} = \text{CH}_2\text{Ph}$)



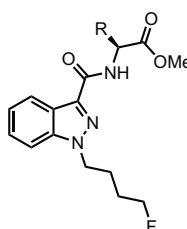
AB-4F-BUTINACA (28: $\text{R} = \text{CH}(\text{CH}_3)_2$)
 ADB-4F-BUTINACA (29: $\text{R} = \text{C}(\text{CH}_3)_3$)
 APP-4F-BUTINACA (30: $\text{R} = \text{CH}_2\text{Ph}$)



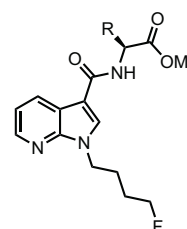
AB-4F-BUT7AICA (31: $\text{R} = \text{CH}(\text{CH}_3)_2$)
 ADB-4F-BUT7AICA (32: $\text{R} = \text{C}(\text{CH}_3)_3$)
 APP-4F-BUT7AICA (33: $\text{R} = \text{CH}_2\text{Ph}$)



MMB-4F-BUTICA (34: $\text{R} = \text{CH}(\text{CH}_3)_2$)
 MDMB-4F-BUTICA (7: $\text{R} = \text{C}(\text{CH}_3)_3$)
 MPP-4F-BUTICA (35: $\text{R} = \text{CH}_2\text{Ph}$)



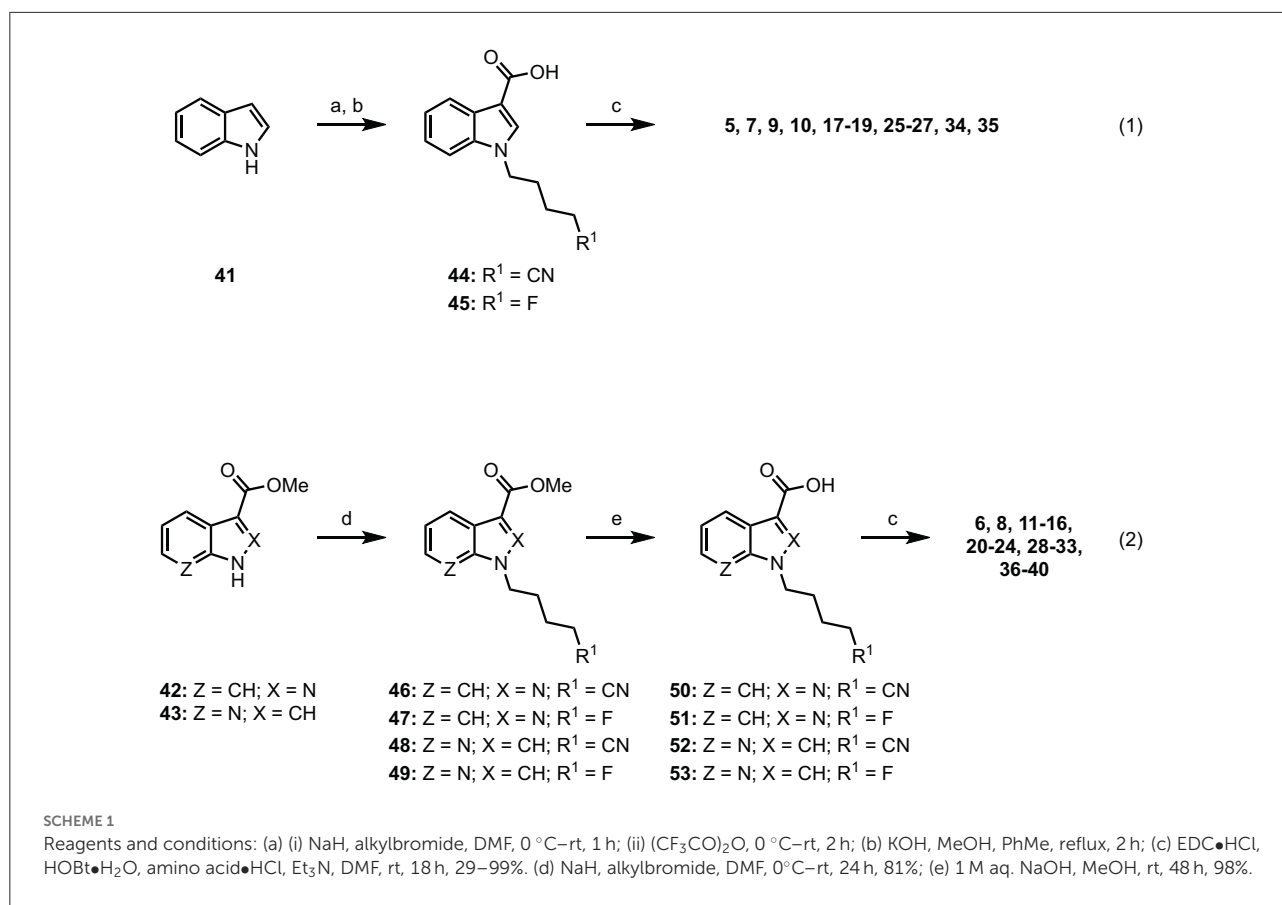
MMB-4F-BUTINACA (36: $\text{R} = \text{CH}(\text{CH}_3)_2$)
 MDMB-4F-BUTINACA (8: $\text{R} = \text{C}(\text{CH}_3)_3$)
 MPP-4F-BUTINACA (37: $\text{R} = \text{CH}_2\text{Ph}$)



MMB-4F-BUT7AICA (38: $\text{R} = \text{CH}(\text{CH}_3)_2$)
 MDMB-4F-BUT7AICA (39: $\text{R} = \text{C}(\text{CH}_3)_3$)
 MPP-4F-BUT7AICA (40: $\text{R} = \text{CH}_2\text{Ph}$)

FIGURE 3

Structures of amino acid-derived 4-cyanobutyl and 4-fluorobutyl-substituted indole, indazole and 7-azaindole SCRAs explored in this study. AB, [(S)-2-amino-3-methylbutanamide]; ADB, [(S)-2-amino-3,3-dimethylbutanamide]; APP, [(S)-2-amino-3-phenylpropanamide]; MMB, [methyl (S)-2-amino-3-methylbutanoate]; MDMB, [methyl (S)-2-amino-3,3-dimethylbutanoate]; MPP, [methyl ((S)-2-amino-3-phenylpropanoate)]; 4-CN-BUT, 4-cyanobutyl; 4F-BUT, 4-fluorobutyl; ICA, indole-3-carboxamide; INACA, indazole-3-carboxamide; 7AICA, 7-aza-indole-3-carboxamide.



THC ($pEC_{50} = 6.76 \pm 0.09$ and $E_{max} = 58\% \pm 3\%$ at CB₁, and $32\% \pm 1\%$ at $30 \mu M$ at CB₂) (36). Potency compared with THC is also similar ($pK_i = 8.09 \pm 0.02$ and 7.50 ± 0.07 at CB₁ and CB₂, respectively) (70).

Effect of 4-cyanobutyl and 4-fluorobutyl substituents on CB₁ and CB₂ activation

Of the 3 chemical modifications investigated in the present study, variation of the tail substituent had the least significant impact on potency and efficacy. The 4-cyanobutyl and 4-fluorobutyl derivatives commonly displayed similar potency at both CB₁ and CB₂, for example in the *tert*-leucinate subgroup (18, 20, 23 \approx 7, 8, 39, respectively), or conversely, exhibited differing potency with no discernable preference for either tail group. Indeed, both tail substituents produced active ligands with sub-nanomolar potency for CB₁ (20: $pEC_{50} = 9.14 \pm 0.14$; 8: $pEC_{50} = 9.39 \pm 0.17$) and low nanomolar potency for CB₂ (20: $pEC_{50} = 8.45 \pm 0.07$; 8: $pEC_{50} = 8.48 \pm 0.14$). These data are consistent with the corresponding structure-affinity trends; however, binding is not predictive of relative potency in some cases. For example, MDMB-4F-BUTINACA (8) exhibits

activation ($pEC_{50} = 9.39 \pm 0.17$) an order of magnitude greater than its affinity ($pK_i = 8.21 \pm 0.13$) for CB₁, whilst for CB₂, the opposite is true ($pEC_{50} = 8.48 \pm 0.14$; $pK_i = 9.92 \pm 0.09$).

Effect of indole, indazole and 7-azaindole core on CB₁ and CB₂ activation

In the present study, the nature of the heterocyclic core greatly impacts potency, giving rise to the same trends as previously documented (51, 54, 71). Rank order potency of activity at CB₁ closely mirrored the observed binding affinities, whereby indazoles ($pEC_{50} = 9.39 \pm 0.17$ – 6.31 ± 0.05) demonstrated equal or greater potency to the corresponding indoles ($pEC_{50} = 8.57 \pm 0.13$ – <5), which were, again, more potent than the corresponding 7-azaindoles ($pEC_{50} = 8.05 \pm 0.21$ – <5). In all cases, the indazole core was required to produce sub-nanomolar potency ($pEC_{50} = 9.39 \pm 0.17$, 9.48 ± 0.14 , 9.14 ± 0.14) observed for compounds 8, 12, and 20, respectively. While the same general trend is realized for activation of CB₂ (indazoles: $pEC_{50} = 8.75 \pm 0.03$ – 7.00 ± 0.36 ; indoles: $pEC_{50} = 8.54 \pm 0.05$ – 6.49 ± 0.2 ; 7-azaindoles: $pEC_{50} = 8.41 \pm 0.08$ – 5.92 ± 0.16), differentiation of heterocyclic cores is less pronounced

TABLE 1 Affinities and functional activities of 4-cyanobutyl derived SCRA at hCB₁ and hCB₂.

Compound	hCB ₁			hCB ₂		
	pK _i ± SEM (K _i , nM)	pEC ₅₀ ± SEM (EC ₅₀ , nM)	E _{max} ± SEM (% CP55,940)	pK _i ± SEM (K _i , nM)	pEC ₅₀ ± SEM (EC ₅₀ , nM)	E _{max} ± SEM (% CP55,940)
AB-4CN-BUTICA (5)	6.26 ± 0.09 (550)	6.40 ± 0.08 (400)	111 ± 5	6.22 ± 0.13 (603)	7.12 ± 0.05 (75.9)	100 ± 2
ADB-4CN-BUTICA (9)	8.17 ± 0.12 (6.8)	7.99 ± 0.16 (10.2)	115 ± 5	8.26 ± 0.06 (5.5)	7.98 ± 0.21 (10.4)	106 ± 6
APP-4CN-BUTICA (10)	5.48 ± 0.11 (3310)	DNC ^b	85 ± 3 ^d	6.11 ± 0.06 (776)	7.01 ± 0.08 (98.4)	95 ± 3
AB-4CN-BUTINACA (11)	7.36 ± 0.12 (43.7)	7.58 ± 0.14 (26.3)	111 ± 5	7.62 ± 0.07 (24.0)	8.30 ± 0.05 (4.97)	103 ± 1
ADB-4CN-BUTINACA (12)	8.09 ± 0.03 (8.13)	9.48 ± 0.14 (0.33)	109 ± 2	8.59 ± 0.05 (2.57)	8.75 ± 0.03 (1.76)	96 ± 2
APP-4CN-BUTINACA (13)	5.97 ± 0.09 (1100)	DNC ^b	104 ± 3 ^d	6.78 ± 0.03 (170)	7.13 ± 0.25 (74.1)	107 ± 11
AB-4CN-BUT7AICA (14)	5.59 ± 0.12 (2570)	DNC ^b	80 ± 3 ^d	5.49 ± 0.03 (3240)	6.41 ± 0.10 (390)	87 ± 5
ADB-4CN-BUT7AICA (15)	6.81 ± 0.09 (155)	7.85 ± 0.1 (14.0)	102 ± 4	6.84 ± 0.10 (145)	8.22 ± 0.03 (6.09)	96 ± 1
APP-4CN-BUT7AICA (16)	< 5	ND ^c	25 ± 3 ^d	5.73 ± 0.08 (1860)	6.64 ± 0.09 (232)	72 ± 3
MMB-4CN-BUTICA (17)	6.80 ± 0.14 (159)	7.29 ± 0.06 (50.8)	105 ± 3	7.07 ± 0.12 (85.1)	7.87 ± 0.08 (13.5)	95 ± 3
MDMB-4CN-BUTICA (18)	8.18 ± 0.11 (6.61)	8.57 ± 0.13 (2.68)	111 ± 3	8.69 ± 0.05 (2.04)	8.39 ± 0.14 (4.04)	101 ± 4
MPP-4CN-BUTICA (19)	7.07 ± 0.09 (85.1)	7.45 ± 0.07 (35.5)	109 ± 3	8.06 ± 0.02 (8.71)	8.07 ± 0.08 (8.44)	105 ± 3
MMB-4CN-BUTINACA (6)	7.76 ± 0.06 (17.4)	8.44 ± 0.19 (3.61)	117 ± 6	8.19 ± 0.14 (6.46)	8.67 ± 0.17 (2.14)	101 ± 4
MDMB-4CN-BUTINACA (20)	8.89 ± 0.09 (1.29)	9.14 ± 0.14 (0.72)	113 ± 2	9.53 ± 0.07 (0.295)	8.45 ± 0.07 (3.56)	101 ± 2
MPP-4CN-BUTINACA (21)	7.68 ± 0.13 (20.9)	8.06 ± 0.07 (8.72)	115 ± 3	8.42 ± 0.10 (3.80)	8.49 ± 0.06 (3.24)	100 ± 2
MMB-4CN-BUT7AICA (22)	5.82 ± 0.08 (1510)	6.37 ± 0.1 (430)	114 ± 7	6.50 ± 0.07 (316)	7.17 ± 0.08 (68.3)	95 ± 4
MDMB-4CN-BUT7AICA (23)	8.03 ± 0.13 (9.2)	7.99 ± 0.16 (10.3)	114 ± 5	8.61 ± 0.08 (2.4)	7.90 ± 0.16 (12.6)	106 ± 5
MPP-4CN-BUT7AICA (24)	6.42 ± 0.07 (380)	6.73 ± 0.08 (189)	110 ± 5	7.26 ± 0.06 (55.0)	7.84 ± 0.05 (14.3)	104 ± 2

^aData represent mean values ± standard error of the mean (SEM) from 3 to 6 independent experiments;

^bDid not converge (DNC);

^cNot determined (ND): <50% change in fluorescence at 10 μM;

^dMaximal response at 10 μM.

AB, [(S)-2-amino-3-methylbutanamide]; ADB, [(S)-2-amino-3,3-dimethylbutanamide]; APP, [(S)-2-amino-3-phenylpropanamide]; MMB, [methyl (S)-2-amino-3-methylbutanoate]; MDMB, [methyl (S)-2-amino-3,3-dimethylbutanoate]; MPP, methyl [(S)-2-amino-3-phenylpropanoate]; 4-CN-BUT, 4-cyanobutyl; 4F-BUT, 4-fluorobutyl; ICA, indole-3-carboxamide; INACA, indazole-3-carboxamide; 7AICA, 7-aza-indole-3-carboxamide.

for this receptor, with the MPP subgroup (21 > 19 > 24) highlighting this effect. Notably, this is not apparent for MDMB derivatives (7 ≈ 8 ≈ 39), whereby all core motifs conferred similar potency.

Effect of amino acid derived head groups on CB₁ and CB₂ activation

As described previously, *tert*-leucine derived compounds (MDMB/ADB) are commonly more potent than the corresponding valine (ADB/AB) species at CB₁, despite differing only by a single methyl group (36, 51, 54, 69, 71, 72). In line with this is the greater potencies of MDMB/ADB vs. MMB/AB analogs for indole (18, 9 > 5, 17), indazole (20, 12 > 6, 11) and 7-azaindole (23, 15 > 22, 14) sub-groups observed

here. Further, MDMB- and ADB-4F-BUTINACA (8 and 29) represent two of only three substrates with sub-nanomolar potency, and indeed the highest potencies observed for CB₁. While the methyl esters of phenylalanine (MPP) were commonly equipotent or greater than valine (AB and MMB) analogs, unlike with *tert*-leucine derivatives, switching to the terminal amide (APP) was detrimental to potency at CB₁. Specifically, when combined with an indole (10 and 27) or 7-azaindole core (16 and 33), the APP substituent produced submaximal agonist activity at the highest concentration tested (10 μM), whereas full efficacy was maintained with the indazole core (i.e., 13: E_{max} = 104%). In terms of CB₂, structure-activity trends align closely with CB₁; however, with all phenylalaninamides (APP) except APP-4CN-BUT7AICA (16: E_{max} = 73%, pEC₅₀ = 6.63 ± 0.11) having full agonist effect with moderate potency. As with binding, these findings indicate a CB₂ receptor subtype

TABLE 2 Affinities and functional activities of 4-fluorobutyl derived SCRA at hCB₁ and hCB₂.

Compound	hCB ₁			hCB ₂		
	pK _i ± SEM (K _i , nM)	pEC ₅₀ ± SEM (EC ₅₀ , nM)	E _{max} ± SEM (% CP55,940)	pK _i ± SEM (K _i , nM)	pEC ₅₀ ± SEM (EC ₅₀ , nM)	E _{max} ± SEM (% CP55,940)
AB-4F-BUTICA (25)	6.00 ± 0.11 (1,000)	7.02 ± 0.05 (96.5)	108 ± 3	7.09 ± 0.08 (82)	7.63 ± 0.05 (23.5)	97 ± 2
ADB-4F-BUTICA (26)	7.46 ± 0.08 (35)	7.39 ± 0.09 (40.4)	110 ± 4	8.10 ± 0.11 (8.0)	7.36 ± 0.12 (44.1)	105 ± 4
APP-4F-BUTICA (27)	5.50 ± 0.10 (3,200)	DNC ^b	82 ± 4 ^d	6.76 ± 0.01 (170)	6.51 ± 0.16 (306)	108 ± 8
AB-4F-BUTINACA (28)	6.88 ± 0.13 (130)	8.22 ± 0.06 (5.98)	107 ± 2	8.07 ± 0.07 (8.5)	8.31 ± 0.04 (4.85)	96 ± 1
ADB-4F-BUTINACA (29)	8.39 ± 0.08 (4.07)	8.79 ± 0.06 (1.61)	116 ± 2	9.16 ± 0.04 (0.69)	8.28 ± 0.07 (5.28)	103 ± 2
APP-4F-BUTINACA (30)	5.86 ± 0.13 (1,380)	6.30 ± 0.05 (504)	103 ± 3	7.55 ± 0.15 (28.2)	8.08 ± 0.13 (8.35)	101 ± 12
AB-4F-BUT7AICA (31)	<5	DNC ^b	82 ± 4 ^d	5.86 ± 0.07 (1,400)	6.86 ± 0.05 (137)	98 ± 4
ADB-4F-BUT7AICA (32)	5.90 ± 0.06 (1,300)	7.34 ± 0.13 (46.0)	112 ± 6	7.34 ± 0.06 (46)	8.30 ± 0.04 (4.99)	108 ± 2
APP-4F-BUT7AICA (33)	<5	ND ^c	25 ± 14 ^d	5.62 ± 0.04 (2,400)	5.93 ± 0.16 (1,170)	99 ± 12
MMB-4F-BUTICA (34)	7.01 ± 0.10 (97.7)	7.11 ± 0.04 (76.9)	116 ± 3	7.57 ± 0.05 (26.9)	7.95 ± 0.05 (11.4)	102 ± 2
MDMB-4F-BUTICA (7)	7.88 ± 0.12 (13.2)	8.47 ± 0.08 (3.43)	114 ± 3	9.30 ± 0.12 (0.35)	8.54 ± 0.05 (2.87)	110 ± 3
MPP-4F-BUTICA (35)	6.57 ± 0.10 (270)	7.44 ± 0.06 (36.6)	105 ± 2	8.22 ± 0.06 (6.1)	8.00 ± 0.05 (10.1)	100 ± 2
MMB-4F-BUTINACA (36)	7.50 ± 0.15 (32)	8.41 ± 0.08 (3.93)	103 ± 2	8.81 ± 0.09 (1.6)	8.42 ± 0.08 (3.76)	100 ± 2
MDMB-4F-BUTINACA (8)	8.21 ± 0.13 (6.2)	9.39 ± 0.17 (0.41)	106 ± 3	9.92 ± 0.09 (0.10)	8.48 ± 0.14 (3.28)	103 ± 5
MPP-4F-BUTINACA (37)	7.47 ± 0.13 (34)	8.25 ± 0.12 (5.62)	106 ± 3	9.34 ± 0.05 (0.50)	8.33 ± 0.10 (4.65)	101 ± 3
MMB-4F-BUT7AICA (38)	6.65 ± 0.05 (220)	5.86 ± 0.18 (1,390)	115 ± 16	7.22 ± 0.02 (61)	7.30 ± 0.13 (49.6)	114 ± 6
MDMB-4F-BUT7AICA (39)	6.97 ± 0.08 (107)	7.65 ± 0.08 (22.2)	109 ± 3	8.67 ± 0.07 (2.14)	8.41 ± 0.08 (3.88)	95 ± 2
MPP-4F-BUT7AICA (40)	6.06 ± 0.13 (880)	6.20 ± 0.14 (637)	122 ± 10	7.54 ± 0.08 (29)	7.57 ± 0.17 (26.9)	110 ± 6

^aData represent mean values ± standard error of the mean (SEM) from 3 to 6 independent experiments;

^bDid not converge (DNC);

^cNot determined (ND): <50% change in fluorescence at 10 μM;

^dMaximal response at 10 μM.

AB, [(S)-2-amino-3-methylbutanamide]; ADB, [(S)-2-amino-3,3-dimethylbutanamide]; APP, [(S)-2-amino-3-phenylpropanamide]; MMB, [methyl (S)-2-amino-3-methylbutanoate]; MDMB, [methyl (S)-2-amino-3,3-dimethylbutanoate]; MPP, methyl [(S)-2-amino-3-phenylpropanoate]; 4-CN-BUT, 4-cyanobutyl; 4F-BUT, 4-fluorobutyl; ICA, indole-3-carboxamide; INACA, indazole-3-carboxamide; 7AICA, 7-aza-indole-3-carboxamide.

selectivity for the phenylalaninamide group. In general, the SARs described here corroborate the observed structure-affinity trends for the compounds in the present study, as well as those previously found (54).

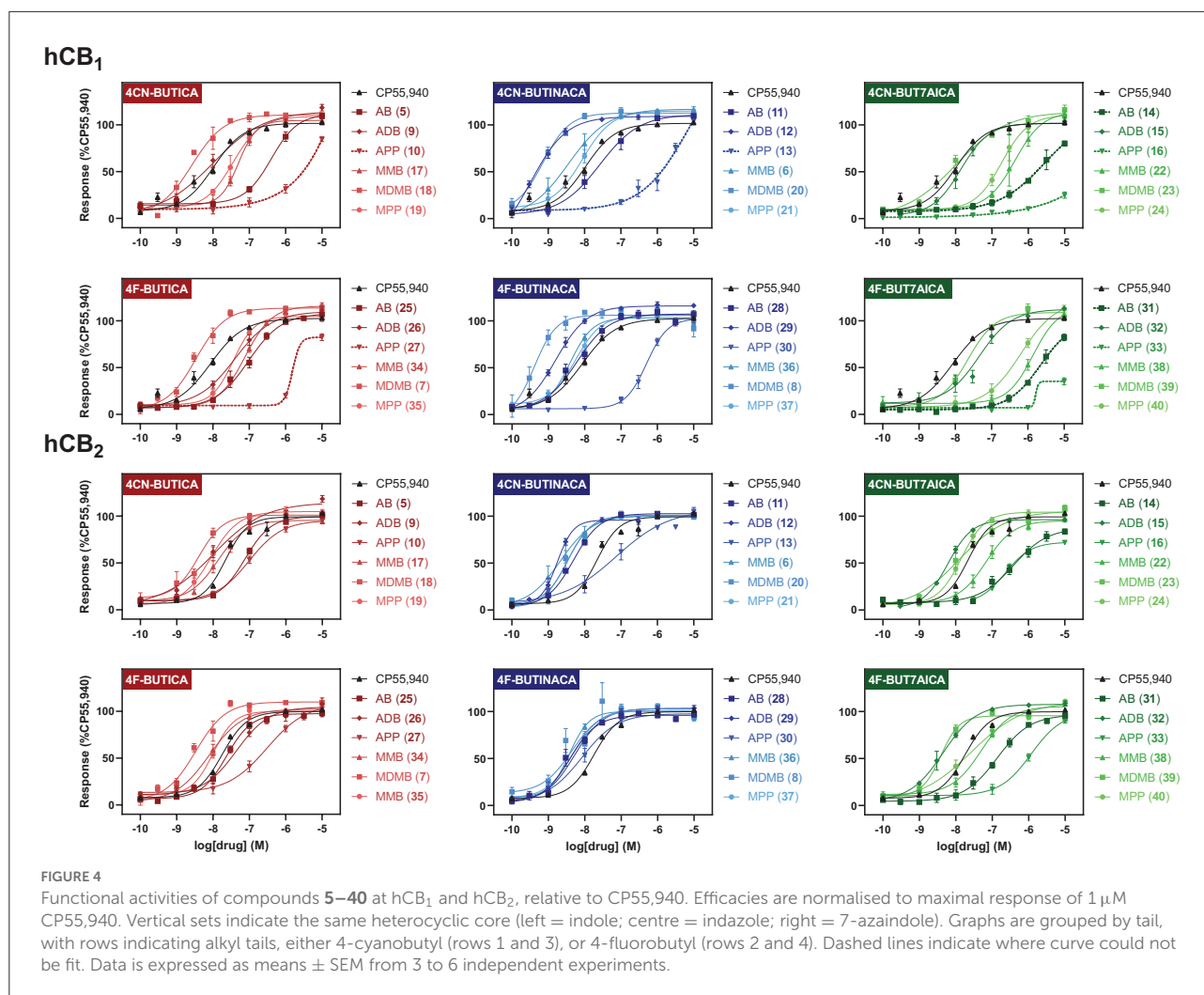
In silico molecular docking study

To rationalize the novel SARs observed *in vitro* at CB₁ and CB₂, we performed docking for each of the screened ligands using the cryo-EM structures of the CB₁ (PDB ID: 6N4B) and the CB₂ (PDB ID: 6PT0) receptors retrieved from the Research Collaboratory for Structural Bioinformatics Protein Databank (RCSB PDB) (57–59). These agonist-bound structures were chosen for the similarity between our compounds and the cognate ligands MDMB-FUBINACA (6N4B) and WIN 55,212-2 (6PT0).

When docking at CB₁ there were π-π interactions between each of the ligands and residues PHE200 and PHE268. The

flexible 4-fluorobutyl and 4-cyanobutyl tail groups occupied a hydrophobic pocket comprised of MET363, LEU276, TYR275, LEU193, and ILE271. There is also a common polar interaction between the amide linker carbonyl and SER383, as well as the terminal carbonyl and HIE178.

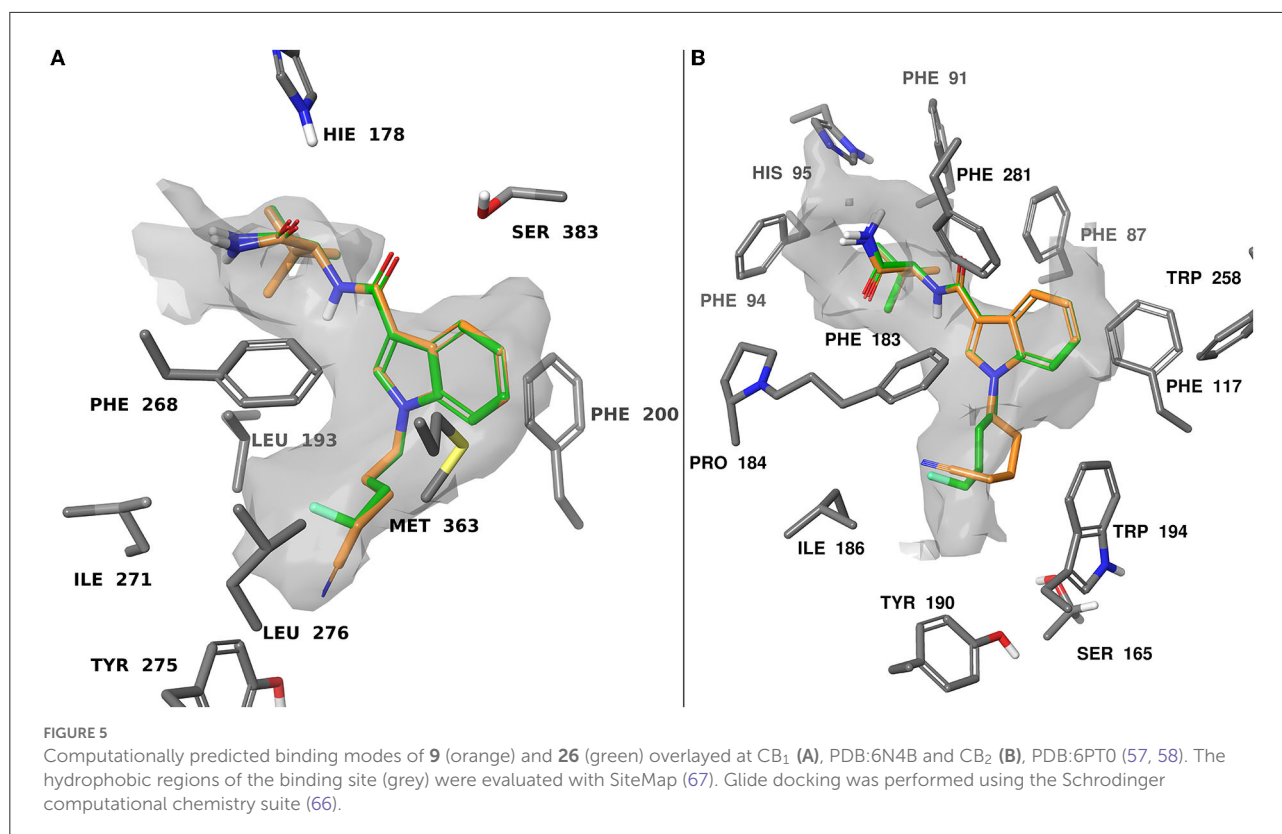
Docking at CB₂ was dictated by hydrophobic interactions between the core and PHE117, and PHE183 residues. The flexible tail occupied a pocket comprised of TRP194, ILE186, TYR190, and SER165. The amide and ester head groups occupied a pocket comprised of PHE91, PHE94, HIS95, and PRO184. Ligands bearing a terminal amide had the potential for H-bonding with the backbone carbonyl of PHE183. Pairs of docking poses for ligands that differed by tail substitution were selected for strain rescoring (see SI, figures S105–116 for all calculated docking poses). This allowed us to investigate the SAR described in the *in vitro* section, wherein many 4-fluorobutyl ligands showed higher affinity for the CB₂ receptor than their 4-cyanobutyl counterparts. Given the lack of formal intermolecular interactions possible for this substituent, the



effect is likely due to the size-constraints of the binding pocket for CB₂ as compared with CB₁. Figure 5 shows an overlay of compounds 9 and 26 at both CB₁ and CB₂, as well as the computed hydrophobic regions of the binding site. Relative to CB₁, the CB₂ binding site region occupied by the 4-fluorobutyl or 4-cyanobutyl tail is significantly constrained. This was observed by Sitemap calculation on the active site of CB₁ and CB₂ receptors as illustrated in Figure 5. This may force the longer and more rigid 4-cyanobutyl tail into a higher strain conformation to adopt the predicted binding pose. The strain energy of the ligands in their bound state relative to their unbound state was calculated, and the values compared for analogous ligands (see SI Table T1). The mean difference and standard error between the docked 4-cyanobutyl and 4-fluorobutyl ligands were 0.220 ± 0.400 kcal/mol at CB₁ and 2.552 ± 0.468 kcal/mol at CB₂.

Conclusions

The detected SCRA AB-4CN-BUTICA, MMB-4CN-BUTINACA, MDMB-4F-BUTICA, MDMB-4F-BUTINACA, as well as a series of 32 analogs, were synthesized, characterized, and evaluated *in vitro* using a radioligand binding assay and a functional membrane potential assay at both human CB₁ and CB₂. These data confirm that AB-4CN-BUTICA, MMB-4CN-BUTINACA, MDMB-4F-BUTICA, MDMB-4F-BUTINACA are potent and efficacious cannabinoid receptor ligands. Most analogs in the present study, barring the APP (phenylalaninamide) derivatives, were also potent and efficacious cannabinoid ligands. SAR trends observed here were consistent with those previously described for with respect to head group and core group contributions to ligand activity (30, 36, 50, 54, 69, 72). The increased affinity for



4-fluorobutyl derivatives at CB₂ is likely to arise from increased strain of the 4-cyanobutyl tail in the hydrophobic tail pocket. Given these pharmacological data, availability of precursory chemical building blocks, ease of synthesis, and structural similarity to previous SCRAs, the compounds evaluated in this study should be monitored as potential emerging NPS in the marketplace.

Data availability statement

The original contributions presented in the study are included in the article/Supplementary material, further inquiries can be directed to the corresponding author/s.

Author contributions

ES and JL synthesized and characterized compounds under the supervision of AA and SB. *In vitro* binding data were obtained by SC under the supervision of MG. *In vitro* functional characterization was performed by RB and CF under the supervision of EC and by TF and HZ under the supervision of MS and MC. *In silico* docking experiments were performed by JM under the supervision of FL and DH. HRMS data were obtained by RE under the supervision of RG. ES, JM, IM, EC, MC, MG, AA, and SB conceived the

experiments. ES, JM, EC, AA, and SB wrote the manuscript. All authors reviewed drafts of the manuscript and approved the final version.

Funding

Parts of this work were supported NHMRC Project Grant 1161571 and Brain and Mind Centre Research Development Grant awarded to SB. ES, RB, JM, CF, IM, EC, AA, and SB are supported by the Lambert Initiative for Cannabinoid Therapeutics, a philanthropic research program based at the University of Sydney. ES, JM, and TF are supported by an Australian Government Research Training Scholarships through the University of Sydney and Macquarie University respectively.

Acknowledgments

This research was facilitated by access to Sydney Mass Spectrometry, a core research facility at the University of Sydney, with the authors acknowledging Chianna Dane for obtaining several HRMS spectra. The authors would like to thank Rebecca Gordon and Dr. Richard Kevin from the Lambert Initiative for Cannabinoid Therapeutics for obtaining

LCMS and UV spectra. The authors from the University of Sydney would like to acknowledge the Gadigal people of the Eora Nation as the traditional custodians of the land on which they work, and where this research was conducted. These authors would like to pay their respects those who have cared and continue to care for Country, to elders past, present, and emerging.

Conflict of interest

The authors declare that the research was conducted in the absence of any commercial or financial relationships that could be construed as a potential conflict of interest.

References

1. UNODC. *World Drug Report 2021* (2021).
2. Halter S, Mogler L, Auwarter V. Quantification of herbal mixtures containing Cumyl-PEGACLONE-is inhomogeneity still an issue? *J Anal Toxicol.* (2020) 44:81–5. doi: 10.1093/jat/bkz028
3. Brandehoff N, Adams A, McDaniel K, Banister SD, Gerona R, Monte AA. Synthetic cannabinoid “Black Mamba” infidelity in patients presenting for emergency stabilization in Colorado: a P SCAN Cohort. *Clin Toxicol.* (2018) 56:193–8. doi: 10.1080/15563650.2017.1357826
4. Gatch MB, Forster MJ. Delta9-Tetrahydrocannabinol-like effects of novel synthetic cannabinoids found on the gray market. *Behav Pharmacol.* (2015) 26:460–8. doi: 10.1097/FBP.0000000000000150
5. Worob A, Wenthur C. DARK Classics in Chemical Neuroscience: synthetic cannabinoids (Spice/K2). *ACS Chem Neurosci.* (2019) 11:3881–92. doi: 10.1021/acchemneuro.9b00586
6. Banister SD, Arnold JC, Connor M, Glass M, McGregor IS. Dark classics in chemical neuroscience: delta(9)-tetrahydrocannabinol. *ACS Chem Neurosci.* (2019) 10:2160–75. doi: 10.1021/acchemneuro.8b00651
7. Van Rafelghem B, Covaci A, Anseeuw K, van Nuijs ALN, Neels H, Mahieu B, et al. Suicide by vaping the synthetic cannabinoid 4F-MDMB-BINACA: cannabinoid receptors and fluoride at the crossroads of toxicity? *Forensic Sci Med Pathol.* (2021) 17:684–8. doi: 10.1007/s12024-021-00424-7
8. Manini AF, Krotulski AJ, Schimmel J, Allen L, Hurd YL, Richardson LD, et al. Respiratory failure in confirmed synthetic cannabinoid overdose. *Clin Toxicol.* (2021) 60:524–26. doi: 10.1080/15563650.2021.1975734
9. Hermanns-Clausen M, Muller D, Kithinji J, Angerer V, Franz F, Eyer F, et al. Acute side effects after consumption of the new synthetic cannabinoids AB-CHMINACA and MDMB-CHMICA. *Clin Toxicol.* (2018) 56:404–11. doi: 10.1080/15563650.2017.1393082
10. Kusano M, Zaitis K, Taki K, Hisatsune K, Nakajima J, Moriyasu T, et al. Fatal intoxication by 5F-ADB and diphenidine: detection, quantification, and investigation of their main metabolic pathways in humans by LC/MS/MS and LC/Q-TOFMS. *Drug Test Anal.* (2018) 10:284–93. doi: 10.1002/dta.2215
11. Giorgetti A, Busardo FP, Tittarelli R, Auwarter V, Giorgetti R. Post-mortem toxicology: a systematic review of death cases involving synthetic cannabinoid receptor agonists. *Front Psychiatry.* (2020) 11:464. doi: 10.3389/fpsy.2020.00464
12. Lam RPK, Tang MHY, Leung SC, Chong YK, Tsui MSH, Mak TWL. Supraventricular tachycardia and acute confusion following ingestion of e-cigarette fluid containing AB-FUBINACA and ADB-FUBINACA: a case report with quantitative analysis of serum drug concentrations. *Clin Toxicol.* (2017) 55:662–7. doi: 10.1080/15563650.2017.1307385
13. Papadopoulos EA, Cummings KR, Marraffa JM, Aldous KM, Li L, Ahmad N. Reports of adverse health effects related to synthetic cannabinoid use in New York State. *Am J Addict.* (2017) 26:772–5. doi: 10.1111/ajad.12636
14. Sampson CS, Bedy SM, Carlisle T. Withdrawal seizures seen in the setting of synthetic cannabinoid abuse. *Am J Emerg Med.* (2015) 33:1712 e3. doi: 10.1016/j.ajem.2015.03.025
15. Schep LJ, Slaughter RJ, Hudson S, Place R, Watts M. Delayed seizure-like activity following analytically confirmed use of previously unreported synthetic cannabinoid analogues. *Hum Exp Toxicol.* (2015) 34:557–60. doi: 10.1177/0960327114550886
16. Schwartz MD, Trecki J, Edison LA, Steck AR, Arnold JK, Gerona RR. A common source outbreak of severe delirium associated with exposure to the novel synthetic cannabinoid ADB-PINACA. *J Emerg Med.* (2015) 48:573–80. doi: 10.1016/j.jemermed.2014.12.038
17. Thornton SL, Akpunonu P, Glauner K, Hoehn KS, Gerona R. Unintentional pediatric exposure to a synthetic cannabinoid (AB-PINACA) resulting in coma and intubation. *Ann Emerg Med.* (2015) 66:343–4. doi: 10.1016/j.annemergmed.2015.05.021
18. Tyndall JA, Gerona R, De Portu G, Trecki J, Elie MC, Lucas J, et al. An outbreak of acute delirium from exposure to the synthetic cannabinoid AB-CHMINACA. *Clin Toxicol.* (2015) 53:950–6. doi: 10.3109/15563650.2015.1100306
19. Cooper ZD. Adverse effects of synthetic cannabinoids: management of acute toxicity and withdrawal. *Curr Psychiatry Rep.* (2016) 18:52. doi: 10.1007/s11920-016-0694-1
20. Barcelo B, Pichini S, Lopez-Corominas V, Gomila I, Yates C, Busardo FP, et al. Acute intoxication caused by synthetic cannabinoids 5F-ADB and MMB-2201: A case series. *Forensic Sci Int.* (2017) 273:e10–14. doi: 10.1016/j.forsciint.2017.01.020
21. Louh IK, Freeman WD. A ‘spicy’ encephalopathy: synthetic cannabinoids as cause of encephalopathy and seizure. *Crit Care.* (2014) 18:553. doi: 10.1186/s13054-014-0553-6
22. Adamowicz P. Fatal intoxication with synthetic cannabinoid MDMB-CHMICA. *Forensic Sci Int.* (2016) 261:e5–10. doi: 10.1016/j.forsciint.2016.02.024
23. Pant S, Deshmukh A, Dholaria B, Kaur V, Ramavaram S, Ukur M, et al. Spicy seizure. *Am J Med Sci.* (2012) 344:67–8. doi: 10.1097/MAJ.0b013e31824cf5c2
24. Schneir AB, Baumbacher T. Convulsions associated with the use of a synthetic cannabinoid product. *J Med Toxicol.* (2012) 8:62–4. doi: 10.1007/s13181-011-0182-2
25. McQuade D, Hudson S, Dargan PI, Wood DM. First European case of convulsions related to analytically confirmed use of the synthetic cannabinoid receptor agonist AM-2201. *Eur J Clin Pharmacol.* (2013) 69:373–6. doi: 10.1007/s00228-012-1379-2
26. Thornton SL, Wood C, Friesen MW, Gerona RR. Synthetic cannabinoid use associated with acute kidney injury. *Clin Toxicol.* (2013) 51:189–90. doi: 10.3109/15563650.2013.770870
27. Buser GL, Gerona RR, Horowitz BZ, Vian KP, Troxell ML, Hendrickson RG, et al. Acute kidney injury associated with smoking synthetic cannabinoid. *Clin Toxicol.* (2014) 52:664–73. doi: 10.3109/15563650.2014.932365

Publisher’s note

All claims expressed in this article are solely those of the authors and do not necessarily represent those of their affiliated organizations, or those of the publisher, the editors and the reviewers. Any product that may be evaluated in this article, or claim that may be made by its manufacturer, is not guaranteed or endorsed by the publisher.

Supplementary material

The Supplementary Material for this article can be found online at: <https://www.frontiersin.org/articles/10.3389/fpsy.2022.1010501/full#supplementary-material>

28. Adams AJ, Banister SD, Irizarry L, Trecki J, Schwartz M, Gerona R. “Zombie” outbreak caused by the synthetic cannabinoid AMB-FUBINACA in New York. *N Engl J Med.* (2017) 376:235–42. doi: 10.1056/NEJMoa1610300
29. Springer YP, Gerona R, Scheunemann E, Shafer SL, Lin T, Banister SD, et al. Increase in adverse reactions associated with use of synthetic cannabinoids - Anchorage, Alaska, 2015–2016. *MMWR Morb Mortal Wkly Rep.* (2016) 65:1108–11. doi: 10.15585/mmwr.mm6540a4
30. Banister SD, Kevin RC, Martin L, Adams A, Macdonald C, Manning JJ, et al. The chemistry and pharmacology of putative synthetic cannabinoid receptor agonist (SCRA) new psychoactive substances (NPS) 5F-PY-PICA, 5F-PY-PINACA, and their analogs. *Drug Test Anal.* (2019) 11:976–89. doi: 10.1002/dta.2583
31. Simon G, Tóth D, Heckmann V, Mayer M, Kuzma M. Simultaneous fatal poisoning of two victims with 4F-MDMB-BINACA and ethanol. *Forensic Toxicol.* 17, 684–8. (2022). doi: 10.1007/s11419-022-00632-y
32. Wilson CD, Hiranita T, Fantegrossi WE. Cannabimimetic effects of abused indazole-carboxamide synthetic cannabinoid receptor agonists AB-PINACA, 5F-AB-PINACA and 5F-ADB-PINACA in mice: tolerance, dependence and withdrawal. *Drug Alcohol Depend.* (2022) 236:109468. doi: 10.1016/j.drugalcdep.2022.109468
33. Huffman JW, Zengin G, Wu MJ, Lu J, Hynd G, Bushell K, et al. Structure-activity relationships for 1-alkyl-3-(1-naphthoyl)indoles at the cannabinoid CB(1) and CB(2) receptors: steric and electronic effects of naphthoyl substituents. New highly selective CB(2) receptor agonists. *Bioorg Med Chem.* (2005) 13:89–112. doi: 10.1016/j.bmc.2004.09.050
34. Dresen S, Ferreiros N, Putz M, Westphal F, Zimmermann R, Auwarter V. Monitoring of herbal mixtures potentially containing synthetic cannabinoids as psychoactive compounds. *J Mass Spectrom.* (2010) 45:1186–94. doi: 10.1002/jms.1811
35. Wiley JL, Marusch JA, Lefever TW, Grabenauer M, Moore KN, Thomas BF. Cannabinoids in disguise: Delta9-tetrahydrocannabinol-like effects of tetramethylcyclopropyl ketone indoles. *Neuropharmacology.* (2013) 75:145–54. doi: 10.1016/j.neuropharm.2013.07.022
36. Banister SD, Moir M, Stuart J, Kevin RC, Wood KE, Longworth M, et al. Pharmacology of indole and indazole synthetic cannabinoid designer drugs AB-FUBINACA, ADB-FUBINACA, AB-PINACA, ADB-PINACA, 5F-AB-PINACA, 5F-ADB-PINACA, ADBICA, and 5F-ADBICA. *ACS Chem Neurosci.* (2015) 6:1546–59. doi: 10.1021/acscchemneuro.5b00112
37. Choi H, Heo S, Kim E, Hwang BY, Lee C, Lee J. Identification of (1-pentylindol-3-yl)-(2,2,3,3-tetramethylcyclopropyl)methanone and its 5-pentyl fluorinated analog in herbal incense seized for drug trafficking. *Forensic Toxicol.* (2013) 31:86–92. doi: 10.1007/s11419-012-0170-5
38. Buchler IP, Hayes MJ, Hegde SG, Hockerman SL, Jones DE, Kortum SW, et al. *Indazole Derivatives Patent WO2009106982A1.* New York, NY: Pfizer Inc. (2009).
39. Auwarter V, Dresen S, Weinmann W, Müller M, Putz M, Ferreiros N. ‘Spice’ and other herbal blends: harmless incense or cannabinoid designer drugs? *J Mass Spectrom.* (2009) 44:832–7. doi: 10.1002/jms.1558
40. Banister SD, Connor M. The chemistry and pharmacology of synthetic cannabinoid receptor agonists as new psychoactive substances: origins. *Handb Exp Pharmacol.* (2018) 252:165–90. doi: 10.1007/164_2018_143
41. Banister SD, Connor M. The chemistry and pharmacology of synthetic cannabinoid receptor agonist new psychoactive substances: evolution. *Handb Exp Pharmacol.* (2018) 252:191–226. doi: 10.1007/164_2018_144
42. Gerona R, Ellison R, Sparkes E, Ametovski A, Fletcher C, Cairns EA, et al. *Announcement of a Newly Identified Synthetic Cannabinoid 4-CN-AMB-BUTINACA.* DEA Tox Announcement (2020). Available online at: https://www.deadiversion.usdoj.gov/dea_tox/4CN-AMB-BUTINACA.pdf (accessed September 1, 2022).
43. Gerona R, Ellison R, Sparkes E, Ametovski A, Chen S, Glass M, et al. *Announcement of a Newly Identified Synthetic Cannabinoid 4CN-AB-BUTICA.* DEA Tox Announcement (2021). Available online at: https://www.deadiversion.usdoj.gov/dea_tox/4CN-AB-BUTICA.pdf (accessed September 1, 2022).
44. Sciensano BEWSDB. *Fact Sheet 4F-MDMB-BICA Methyl 2-(((1-(4-Fluorobutyl)-1H-indol-3-yl)carbonyl)amino)-3,3-Dimethylbutanoate.* Brussels: Sciensano (2020).
45. Krotulski AJ, Mohr ALA, Kacinko SL, Fogarty MF, Shuda SA, Diamond FX, et al. 4F-MDMB-BINACA: a new synthetic cannabinoid widely implicated in forensic casework. *J Forensic Sci.* (2019) 64:1451–61. doi: 10.1111/1556-4029.14101
46. Norman C, McKirdy B, Walker G, Dugard P, NicDaeid N, McKenzie C. Large-scale evaluation of ion mobility spectrometry for the rapid detection of synthetic cannabinoid receptor agonists in infused papers in prisons. *Drug Test Anal.* (2021) 13:644–63. doi: 10.1002/dta.2945
47. Canazza I, Ossato A, Vincenzi F, Gregori A, Di Rosa F, Nigro F, et al. Pharmacotoxicological effects of the novel third-generation fluorinated synthetic cannabinoids, 5F-ADBINACA, AB-FUBINACA, and STS-135 in mice. *In vitro and in vivo studies. Hum Psychopharmacol.* (2017) 32:e2601. doi: 10.1002/hup.2601
48. Haschimi B, Mogler L, Halter S, Giorgetti A, Schwarze B, Westphal F, et al. Detection of the recently emerged synthetic cannabinoid 4F-MDMB-BINACA in “legal high” products and human urine specimens. *Drug Test Anal.* (2019) 11:1377–86. doi: 10.1002/dta.2666
49. Tokarczyk B, Jurczyk A, Krupińska J, Adamowicz P. Fatal intoxication with new synthetic cannabinoids 5F-MDMB-PICA and 4F-MDMB-BINACA—parent compounds and metabolite identification in blood, urine and cerebrospinal fluid. *Forensic Sci Med Pathol.* (2022) 1–10. doi: 10.1007/s12024-022-00492-3
50. Pike E, Grafinger KE, Cannae A, Ametovski A, Luo JL, Sparkes E, et al. Systematic evaluation of a panel of 30 synthetic cannabinoid receptor agonists structurally related to MMB-4en-PICA, MDMB-4en-PINACA, ADB-4en-PINACA, and MMB-4CN-BUTINACA using a combination of binding and different CB1 receptor activation assays: part I—Synthesis, analytical characterization, and binding affinity for human CB1 receptors. *Drug Test Anal.* (2021) 13:1383–401. doi: 10.1002/dta.3037
51. Cannae A, Sparkes E, Pike E, Luo JL, Fang A, Kevin RC, et al. Synthesis and *in vitro* cannabinoid receptor 1 activity of recently detected synthetic cannabinoids 4F-MDMB-BICA, 5F-MPP-PICA, MMB-4en-PICA, CUMYL-CBMICA, ADB-BINACA, APP-BINACA, 4F-MDMB-BINACA, MDMB-4en-PINACA, A-CHMINACA, 5F-AB-P7AICA, 5F-MDMB-P7AICA, and 5F-AP7AICA. *ACS Chem Neurosci.* (2020) 11:4434–46. doi: 10.1021/acscchemneuro.0c00644
52. Finlay DB, Cawston EE, Grimsey NL, Hunter MR, Korde A, Vemuri VK, et al. Gas signalling of the CB1 receptor and the influence of receptor number. *Br J Pharmacol.* (2017) 174:2545–62. doi: 10.1111/bph.13866
53. Grimsey NL, Goodfellow CE, Dragunow M, Glass M. Cannabinoid receptor 2 undergoes Rab5-mediated internalization and recycles via a Rab11-dependent pathway. *Biochim Biophys Acta Mol Cell Res.* (2011) 1813:1554–60. doi: 10.1016/j.bbamcr.2011.05.010
54. Sparkes E, Cairns EA, Kevin RC, Lai F, Grafinger KE, Chen S, et al. Structure-activity relationships of valine, tert-leucine, and phenylalanine amino acid-derived synthetic cannabinoid receptor agonists related to ADB-BUTINACA, APP-BUTINACA, and ADB-P7AICA. *RSC Med Chem.* (2022) 13:156–74. doi: 10.1039/D1MD00242B
55. Knapman A, Santiago M, Du YP, Bennalack PR, Christie MJ, Connor M. A continuous, fluorescence-based assay of mu-opioid receptor activation in AIT-20 cells. *J Biomol Screen.* (2013) 18:269–76. doi: 10.1177/1087057112461376
56. Knapman A, Connor M. Fluorescence-based, high-throughput assays for μ -opioid receptor activation using a membrane potential-sensitive dye. In: Spampinato SM, editor. *Opioid Receptors: Methods and Protocols.* New York, NY: Springer New York (2015). p. 177–85.
57. Krishna Kumar K, Shalev-Benami M, Robertson MJ, Hu H, Banister SD, Hollingsworth SA, et al. Structure of a signaling cannabinoid receptor 1-G protein complex. *Cell.* (2019) 176:448–58 e12. doi: 10.1016/j.cell.2018.11.040
58. Xing C, Zhuang Y, Xu TH, Feng Z, Zhou XE, Chen M, et al. Cryo-EM structure of the human cannabinoid receptor CB2-Gi signaling complex. *Cell.* (2020) 180:645–54 e13. doi: 10.1016/j.cell.2020.01.007
59. Berman HM, Westbrook J, Feng Z, Gilliland G, Bhat TN, Weissig H, et al. The protein data bank. *Nucleic Acids Res.* (2000) 28:235–42. doi: 10.1093/nar/28.1.235
60. Madhavi Sastry G, Adzhigirey M, Day T, Annabhimoju R, Sherman W. Protein and ligand preparation: parameters, protocols, and influence on virtual screening enrichments. *J Comput Aided Mol Des.* (2013) 27:221–34. doi: 10.1007/s10822-013-9644-8
61. Shelley JC, Cholleti A, Frye LL, Greenwood JR, Timlin MR, Uchimaya M. Epik: a software program for pKa prediction and protonation state generation for drug-like molecules. *J Comput Aided Mol Des.* (2007) 21:681–91. doi: 10.1007/s10822-007-9133-z
62. Jacobson MP, Pincus DL, Rapp CS, Day T, Honig B, Shaw DE, et al. A hierarchical approach to all-atom protein loop prediction. *Proteins.* (2004) 55:351–67. doi: 10.1002/prot.10613
63. Olsson MHM, Søndergaard CR, Rostkowski M, Jensen JH. PROPKA3: consistent treatment of internal and surface residues in empirical pKa predictions. *J Chem Theory Comput.* (2011) 7:525–37. doi: 10.1021/ct100578z
64. Lu C, Wu C, Ghoreishi D, Chen W, Wang L, Damm W, et al. OPLS4: improving force field accuracy on challenging regimes of chemical space. *J Chem Theory Comput.* (2021) 17:4291–300. doi: 10.1021/acs.jctc.1c00302
65. LigPrep. *Release 2021-3 ed.* New York, NY: Schrödinger, LLC (2021).

66. Friesner RA, Banks JL, Murphy RB, Halgren TA, Klicic JJ, Mainz DT, et al. Glide: a new approach for rapid, accurate docking and scoring. 1. Method and assessment of docking accuracy. *J Med Chem.* (2004) 47:1739–49. doi: 10.1021/jm0306430
67. Halgren TA. Identifying and characterizing binding sites and assessing druggability. *J Chem Inf Model.* (2009) 49:377–89. doi: 10.1021/ci800324m
68. Ametovski A, Cairns EA, Grafinger KE, Cannaert A, Deventer MH, Chen S, et al. NNL-3: a synthetic intermediate or a new class of hydroxybenzotriazole esters with cannabinoid receptor activity? *ACS Chem Neurosci.* (2021) 12:4020–36. doi: 10.1021/acscchemneuro.1c00348
69. Ametovski A, Macdonald C, Manning JJ, Haneef SAS, Santiago M, Martin L, et al. Exploring stereochemical and conformational requirements at cannabinoid receptors for synthetic cannabinoids related to SDB-006, 5F-SDB-006, CUMYL-PICA, and 5F-CUMYL-PICA. *ACS Chem Neurosci.* (2020) 11:3672–82. doi: 10.1021/acscchemneuro.0c00591
70. Gamage TF, Barrus DG, Kevin RC, Finlay DB, Lefever TW, Patel PR, et al. *In vitro* and *in vivo* pharmacological evaluation of the synthetic cannabinoid receptor agonist EG-018. *Pharmacol Biochem Behav.* (2020) 193:172918. doi: 10.1016/j.pbb.2020.172918
71. Grafinger KE, Cannaert A, Ametovski A, Sparkes E, Cairns E, Banister SD, et al. Systematic evaluation of a panel of 30 synthetic cannabinoid receptor agonists structurally related to MMB-4en-PICA, MDMB-4en-PINACA, ADB-4en-PINACA, and MMB-4CN-BUTINACA using a combination of binding and different CB1 receptor activation assays-Part II: structure activity relationship assessment via a beta-arrestin recruitment assay. *Drug Test Anal.* (2021) 13:1402–11. doi: 10.1002/dta.3035
72. Banister SD, Longworth M, Kevin R, Sachdev S, Santiago M, Stuart J, et al. Pharmacology of valinate and tert-leucinate synthetic cannabinoids 5F-AMBICA, 5F-AMB, 5F-ADB, AMB-FUBINACA, MDMB-FUBINACA, MDMB-CHMICA, and their analogues. *ACS Chem Neurosci.* (2016) 7:1241–54. doi: 10.1021/acscchemneuro.6b00137

Glossary

- [³H]CP55,940, Tritiated 2-((1*R*,2*R*,5*R*)-5-hydroxy-2-(3-hydroxypropyl)cyclohexyl)-5-(2-methyloctan-2-yl)phenol
- AB-4CN-BUTICA, (S)-*N*-(1-amino-3-methyl-1-oxobutan-2-yl)-1-(4-cyanobutyl)-1*H*-indole-3-carboxamide
- ADB-BUTINACA, (S)-*N*-(1-amino-3,3-dimethyl-1-oxobutan-2-yl)-1-butyl-1*H*-indazole-3-carboxamide
- AtT20, Mouse AtT20 FlpIn adenocarcinoma cells
- BSA, Bovine serum albumin
- CB₁, Cannabinoid receptor 1
- CB₂, Cannabinoid receptor 2
- CD₃OD, Deuterated methanol (*d*₄)
- CDCl₃, Deuterated chloroform
- CH₂Cl₂, dichloromethane
- CP55,940, 2-((1*R*,2*R*,5*R*)-5-hydroxy-2-(3-hydroxypropyl)cyclohexyl)-5-(2-methyloctan-2-yl)phenol
- cryo-EM, Cryogenic electron microscopy
- DMEM, Dulbecco's modified eagle medium
- DMF, Dimethylformamide
- DMSO, Dimethyl sulfoxide
- DMSO-*d*₆, Deuterated dimethyl sulfoxide (*d*₆)
- DNC, Did not converge
- EC₅₀, Half maximal effective concentration
- EDC, 1-ethyl-3-(3-dimethylaminopropyl)carbodiimide
- EDTA, Ethylenediaminetetraacetic acid
- E_{max}, Maximum effect
- Et₃N, Triethylamine
- EtOAc, Ethyl acetate
- FBS, Fetal bovine serum
- FTIR, Fourier-transform infrared spectroscopy
- G_{βγ}, G beta-gamma subunit
- GIRK, G protein-coupled inwardly rectifying potassium channel
- HA, Haemagglutinin
- hCB₁, Human cannabinoid receptor 1
- hCB₂, Human cannabinoid receptor 2
- HEK, Human embryonic kidney cells
- HEPES, 2-[4-(2-hydroxyethyl)piperazin-1-yl]ethane-1-sulfonic acid
- HOBt, 1-hydroxybenzotriazole
- HRMS, High resolution mass spectrometry
- JWH-018, Naphthalen-1-yl(1-pentyl-1*H*-indol-3-yl)methanone
- K_d, Equilibrium dissociation constant
- K_i, Inhibition constant
- LC-UV, Liquid chromatography- Ultraviolet
- m.p., Melting point
- MDMB-4F-BUTICA, Methyl (S)-2-(1-(4-fluorobutyl)-1*H*-indole-3-carboxamido)-3,3-dimethylbutanoate
- MDMB-4F-BUTINACA, Methyl (S)-2-(1-(4-fluorobutyl)-1*H*-indazole-3-carboxamido)-3,3-dimethylbutanoate
- MDMB-FUBINACA, Methyl (S)-2-(1-(4-fluorobenzyl)-1*H*-indazole-3-carboxamido)-3,3-dimethylbutanoate
- MeOH, Methanol
- MgSO₄, Magnesium sulfate
- MMB-4CN-BUTINACA, a.k.a. AMB-4CN-BUTINACA, methyl (1-(4-cyanobutyl)-1*H*-indazole-3-carboxyl)-L-valinate
- MS, Mass spectrometry
- Na₂SO₄, Sodium sulfate
- NaH, Sodium hydride
- ND, Not determined
- NMR, Nuclear magnetic resonance
- NPS, New psychoactive substance
- PBS, Phosphate buffered saline
- PEI, Branched polyethyleneimine
- pplss, Preprolactin signal sequence
- RCSB PDB, Research Collaboratory for Structural Bioinformatics Protein Databank
- RMSD, Root-mean-square deviation
- SARs, Structure activity relationships
- SCRA, Synthetic cannabinoid receptor agonist
- SEM, Standard error of the mean
- THC, Δ⁹-tetrahydrocannabinol
- XP, Extra Precision